A CATALOG OF MORPHOLOGICAL TYPES IN
10 DISTANT RICH CLUSTERS OF GALAXIES[*]

Ian Smail[1][†], Alan Dressler[2], Warrick J. Couch[3],
Richard S. Ellis[4], Augustus Oemler Jr.[5][‡], Harvey Butcher[6] & Ray M. Sharples[1].

1) Department of Physics, University of Durham, South Rd, Durham DH1 3LE, UK

2) The Observatories of the Carnegie Institution of Washington, 813 Santa Barbara St., Pasadena, CA 91101-1292

3) School of Physics, University of New South Wales, Sydney 2052, Australia

4) Institute of Astronomy, Madingley Rd, Cambridge CB3 OHA, UK

5) Astronomy Department, Yale University, PO Box 208101, New Haven CT 06520-8101

6) NFRA, PO Box 2, NL-7990, AA Dwingeloo, The Netherlands

ABSTRACT

We present catalogs of objects detected in deep images of 11 fields in 10 distant clusters obtained using WFPC-2 on board the *Hubble Space Telescope*. The clusters span the redshift range $z = 0.37$–0.56 and are the subject of a detailed ground- and space-based study to investigate the evolution of galaxies as a function of environment and epoch. The data presented here include positions, photometry and basic morphological information on ~ 9000 objects in the fields of the 10 clusters. For a brighter subset of 1857 objects in these areas we provide more detailed morphological information.

Subject headings: galaxies: clusters: general – galaxies: evolution – galaxies: structure

---

1. Introduction

Except for the simplest cases, there is significant ambiguity in inferring a galaxy's star formation history from its current integrated properties. However, substantial progress has been made in the study of galaxy evolution through the use of the lookback in cosmic time afforded by observations of distant cluster and field galaxies. Observations of the properties of galaxies at much earlier times can help to distinguish between the possible star formation models and thus offer a clearer picture of the evolutionary paths taken by galaxies as a function of morphology, mass, and environment.

One of the clearest cases of evolution in a galaxy population is that shown by the galaxies in the cores of rich clusters. The surprisingly rapid bluing of this population with increasing redshift was revealed by Butcher & Oemler (BO, 1978, 1984). Spectroscopic surveys of galaxies in these distant clusters (e.g. Couch & Sharples 1987; Dressler & Gunn 1992) uncovered further spectral signatures of evolutionary changes, including high rates of star formation and evidence for strong star bursts. There has been extensive discussion of possible mechanisms for causing the BO effect, although no comprehensive solution has yet been proposed. Nevertheless, it has become apparent that the growth of clusters, with its attendant influx of field galaxies, cannot be viewed in isolation from the changes ongoing in the surrounding field population (e.g. Broadhurst, Ellis & Shanks 1988; Cowie et al. 1996). We are therefore undertaking an ongoing study of the evolution of cluster and supercluster populations at intermediate redshifts to tie the population changes in these environments together and thus provide a unified picture of environmental influences on the evolution of galaxies.

In this paper we present data for the initial study of galaxies in the central regions of rich clusters at intermediate redshifts, observed some 2–$4h^{-1}$ billion years before the present day.[§] Similar studies have been made before (e.g. Butcher & Oemler 1984; Couch & Sharples 1987; Dressler & Gunn 1992), but the advent of the *Hubble Space Telescope* (HST) with its high spatial resolution has added a vital new dimension to the effort — morphological information that can be used to link the evolution of stellar populations with changes in galaxy *structure*, in order to understand how the wide range of galaxies we see today came to be. Pre-refurbishment HST observations by two groups (Couch et al. 1994; Dressler et al. 1994; Oemler et al. 1996) were used in early attempts to correlate spectral evolution with morphological/structural data, and to provide some insight into the mechanisms that might be driving the strong evolution in the cluster galaxy population. These two programs were combined for Cycle-4 into the "MORPHS" project. This program has accumulated post-refurbishment HST images for 11 fields in 10 intermediate redshift ($0.37 < z < 0.56$) clusters. Here we provide the basic data derived from these images, including catalogs of parameters for objects in the fields, and morphological information — both algorithm-derived parameters that provide a rudimentary description of the galaxies, and more detailed visual classification onto the Revised Hubble system. The catalogs, as well as the processed images themselves, are available in CD-ROM form.

[§]We use $q_o = 0.5$ and adopt the dimensionless Hubble parameter, $h = H_o/100$ km sec^{-1} Mpc^{-1}. This geometry means that 1 arcsec is equivalent to 3.09 h^{-1} kpc for our lowest redshift cluster and 3.76 h^{-1} kpc in the most distant.

The catalogs and imaging data, along with the ground-based spectroscopy for galaxies in these fields, form the basis of the analysis which is presented elsewhere. In particular we discuss the morphology-density relation in these distant clusters in Dressler et al. (1996), while the evolution in the cluster spheroidal galaxy populations is addressed in terms of the homogeneity of their colors by Ellis et al. (1996) and through changes in their structural parameters in Barger et al. (1996). An analysis of gravitational lensing by the clusters is given in Smail et al. (1996). Other features of the galaxy populations in these distant clusters, as well as the extensive spectroscopic dataset we have amassed, will be dealt with in forthcoming papers.

A plan of the paper follows. The imaging data on the 11 fields, their reduction and cataloging are discussed in §2. We present the scheme adopted for the morphological classification of brighter subsamples in the clusters in §3. Finally, in §4 we give some basic statistics about the galaxy populations in these distant clusters.

2. Reduction and Analysis

2.1. Observations

The lack of a large, well defined catalog of distant clusters hampers selection of targets for studies of galaxy evolution as a function of lookback time and environment. Therefore, the 10 clusters included in this study were not chosen according to strict criteria, such as X-ray luminosity or optical richness, but rather represent the best studied examples at intermediate redshift, $z \sim 0.5$. The clusters span a wide range in X-ray luminosity (Table 1), optical richness (Fig. 5), and mass (Smail et al. 1996).

All the clusters were imaged using the *Wide Field and Planetary Camera 2* (WFPC-2) on board HST. In total 71 primary spacecraft orbits were allocated in Cycle-4 to image fields in 9 of these clusters. These pointings comprised 7 core regions and 2 pointings on fields around 3–5 arcmin from the cores in 2 clusters (A370 and Cl0939+47). Additional pointings of the centers of 2 more clusters were obtained during the ERO phase of Cycle-4 (10 orbits on Cl0939+47) and through the generosity of Turner and collaborators who provided their imaging of Cl0024+16 (a further 18 orbits). The complete cluster sample thus comprises images of the central regions of 8 clusters, the outer regions of another cluster (A370) and both a center and outer field on the final cluster (Cl0939+47). Details of these, together with relevant observational information (field position, orientation, exposure times and surface brightness limits), are given in Table 1. We also list in Table 1 the number of objects in the full catalog of each field, as well as in the morphological samples. Finally, we list some general information about the clusters, including rest-frame velocity dispersions from Dressler & Gunn (1992)[¶] and Soucail et al. (1988), X-ray luminosities in the

---

[¶]These values have been corrected for errors in the original paper resulting from the use of an incorrect sample size in the calculation of the velocity dispersions.

0.3–3.5 keV band (Castander et al. 1994; Henry et al. 1982; Wang & Stocke 1993; Smail et al. 1996) and reddening.

The filters used for the observations discussed here are F450W (B_{450}), F555W (V_{555}), F702W (R_{702}) and F814W (I_{814}). The individual exposures were generally grouped in sets of 4 single-orbit exposures each offset by 2.0 arcsec to allow for hot pixel rejection. After standard pipeline reduction, the images were aligned using integer pixel shifts and combined using the IRAF/STSDAS task CRREJ. The PC chip was then rebinned to the same linear scale as the WFC and the sky levels in the 4 chips equalized, before assembling them into a mosaic. The mosaicing uses integer pixel shifts to roughly position the 4 chips relative to each other. This is sufficient to align objects lying across the chip boundaries at the < 2 pixel level and has the advantage over a true astrometric mosaic that the data are not resampled. We chose to retain the WFPC-2 color system and hence use the F450W, F555W, F702W and F814W zero points from Table 9 of Holtzman et al. (1995). The actual zero point used in the photometry of each frame is written in the header of the image on the CD-ROM under the keyword MAGZPT. The headers also provide all the standard WFPC-2 pipeline reduction information. The final images cover the central 0.4–0.8 h^{-1} Mpc of the clusters (Plates 1a-k) to a 5σ limiting depth of $I_{814} \simeq 26.0$ or $R_{702} \simeq 27.0$.

2.2.   Constructing Object Catalogs

To catalog faint objects in these frames and measure their shapes we use a modified version of the SExtractor image analysis package (Bertin & Arnouts 1996 and below). We adopt a fixed detection isophote equivalent to $\sim 1.3\sigma$ above the sky, where σ is the average standard deviation of the sky noise in the frames measured pixel to pixel, viz. $\mu_{814} = 25.0$ mag arcsec^{-2} ($\mu_{814} = 24.6$ mag arcsec^{-2} for A370#2 and Cl0939+47#2) or $\mu_{702} = 25.7$ mag arcsec^{-2} for the WFC chips, and a minimum area after convolution with a 0.3 arcsec diameter top-hat filter of 0.12 arcsec^2. For the lower sensitivity PC region we used a detection isophote 1 magnitude brighter than the equivalent WFC value. The object catalogs are all constructed from the reddest passband available for a given cluster (either the F702W or F814W exposures). For those clusters where we have observations in more than one passband we measured the colors for cataloged objects in 1.0 arcsec diameter matched apertures using the IRAF task PHOT. It should be noted that we have applied no reddening corrections to *any* of the photometry published in this paper. However, for reference we list in Table 1 the standard reddening estimates for the fields, these indicate that the correction is only appreciable in a single field (Cl0303+17).

We modified the SExtractor code to calculate two additional parameters: the concentration index (C_1), which is the fraction of an object's light contained in the central 30% of its area as measured in an ellipse aligned with the object and having the same axial ratio (c.f. Abrahams et al. 1995 & Fig. 3); and the contrast index (C_2), which measures the fraction of an object's light contained in the brightest 30% of its pixels. The concentration index is a measure of how centrally peaked an object is, while the contrast index provides a similar measure, but without requiring the light to be centrally concentrated. A comparison of these two indices can thus be used to

determine if an object has a smooth (when the two indices have similar values) or clumpy light distribution (when the contrast exceeds the concentration).

After automated detection and deblending, the object catalogs for each frame were visually inspected and spurious objects (e.g. diffraction spikes) were removed. In addition it was found that on rare occasions the detection routine would fail to catalog a particular galaxy, usually owing to its proximity to another brighter object. For completeness SExtractor was therefore re-run on small regions of the frames centered on these objects with a more vigorous deblending criterion and the cataloged parameters for these "additional" objects added to the full catalogs. Such objects have been flagged in the catalogs by having IDs of 3000 and above. The analysis of our frames provides final catalogs of ~ 800 objects in each of the clusters (Tables 1 and 3 a-k).

3. Morphological Classifications

3.1. Visual Typing

While some basic morphological information is available from parameters in the automated catalogs, it was felt that detailed visual classification of galaxies onto the Revised Hubble scheme is still essential. The uniqueness of the dataset and the high quality information contained in it more than justified the large investment of time required. It is apparent that robust morphological classification relies upon an object's image having sufficiently high signal-to-noise, at the level of at least a few hundred. Thus, not every object in the full catalogs can be reliably classified. We therefore chose to limit the morphological classification to objects brighter than a fixed apparent magnitude, although the signal-to-noise limitation actually sets in over a range of about a magnitude, due to the dispersion in galaxy size and surface brightness. After some experimentation we chose $R_{702} \leq 23.5$ or $I_{814} \leq 23.0$ as the limit beyond which the classifications became unreliable. Here we define unreliable to mean that in more than 20% of cases independent classifiers differed by more than 1 class in assigning Revised Hubble types (including cases where classifiers where unable to assign a type). Typically there are ~ 170 galaxies per cluster (Tables 1 and 4a-k) to these limits, ranging between 116 in the outer field of Cl0939+47, up to 248 for Cl0024+16. These objects are identified on Plates 1a-k.

The assignment of basic morphological types on the Revised Hubble Type system was made by visual inspection of images displayed on a workstation. A purpose written script, running under IRAF and using the XIMTOOL display, stepped through each entry in the catalog brighter than the magnitude limit and displayed a pair of 100×100 pixel grayscale images, stretched at 0–100DN and 0–400DN, using a logarithmic display scaling. We use logarithmic display to mimic the response of the photographic plates, the source material used for the fundamental schemes of galaxy classification. By panning through the lookup table, these display combinations offer a wide dynamic range from outer wisps of low surface brightness to high-surface-brightness core structure, allowing detailed and robust classification of the object morphologies.

Galaxy classifications include four components: (1) Revised Hubble type, (2) disturbance index – the perceived disturbance of the galaxy image, (3) dynamical state – our interpretation of the cause of any observed disturbance and (4) comments. In addition to the standard elliptical type, Morgan's "D" and "cD" types were assigned in some obvious cases, though this has not been done in a rigorous way. Revised Hubble types for spirals were assigned in half-class increments, although it is questionable that there is sufficient information in images sampled at this spatial resolution for such discrimination. Nevertheless, we retained such a system to accommodate the scatter between the various classifiers. Morphological classifications of high redshift galaxies may differ from ground-based observations of nearby systems because of several effects, including (1) limited resolution and low signal-to-noise ratios – particularly for the smaller and fainter objects, (2) $(1 + z)^4$ dimming resulting in the loss of information in the fainter outer regions of galaxies, and (3) differential K corrections between bulges and disks. At present it is unknown how these, or other biases, affect the comparison of classifications of distant galaxies with better resolved, higher signal-to-noise images of nearby galaxies, so caution must be exercised in drawing conclusions that are based on more than rudimentary differences.

S0 galaxies were seldom subtyped because of a similar lack of detail (for example, small nuclear dust lanes). Distinguishing elliptical from face-on S0 galaxies is also challenging, particularly at the signal-to-noise ratio and spatial sampling of these high-redshift galaxy images (see Fig. 4). We have used the classes E/S0 or S0/E to describe these ambiguities rather than to classify actual transition cases (in this we differ from the approach used in the Revised Hubble scheme); the order reflects whether the galaxy was more likely to be an E or S0 in the classifier's opinion. Disk galaxies with obvious bars were so noted, for example, SBab, but again, because of limited spatial sampling, their number is very incomplete and should not be taken as representative of the true fraction of barred versus unbarred galaxies. Those objects not well described by an Revised Hubble type were noted with "?" and those whose images appeared non-stellar but were too small for reliable classification were denoted by "X" for compact.

The visual inspections were used to make two additional assignments other than the revised Hubble type. It was felt that some indication of the disturbance of the galaxy image would be useful and hence each classifier recorded a disturbance index (D): 0 — little or no asymmetry, 1 or 2 — moderate or strong asymmetry, 3 or 4 — moderate or strong distortion. These were intended to be objective judgements independent of the possible reason for the disturbance. Accompanying this was a subjective, interpretive description of the possible cause of the disturbance. For those objects where it seemed warranted the following classes were assigned: I — tidal interaction with a neighbor, M — tidal interaction suggesting a merger, T — tidal feature without obvious cause, or C — chaotic. To the extent that these are subjective and interpretive judgements, they should be viewed with caution. For example, the "merger" category was assigned whenever the structure was noticeably disturbed and one or more apparently tidal tails were present, or in the case of two or more close nuclei in a common envelope, but rarely were these as clear cut examples of mergers such as N4038/9 (the so-called "antenae") where two bodies and two tidal tails are clearly visible.

All clusters were classified by AD and all but Cl1447+23 were classified by WJC. RSE classified Cl0016+16, Cl0054−27 and Cl0412−65, and AO classified Cl0939+39, Cl0024+16 and

Cl1447+23. Merging of the independent classifications was performed by AD using a second IRAF script to redisplay each galaxy and the alternative classifications, allowing him to merge the classification lists. In $\geq 80\%$ of cases to our classification limit the classifiers agreed to one class or better, that is, the difference between an E or S0, or an Sb and Sc (Fig. 1). In these cases the modal class was adopted, or, when only two classifications were available, AD would alternate between the classifiers. In those cases where disagreement was more than one class, AD attempted to identify the cause for the difference and resolve the classification in a consistent manner. In most cases there was sufficient information from the individual classifiers for AD to make an objective resolution, but in a small number of cases the final choice was his alone and hence subjective. Nevertheless, we believe that the uncertainty in this process is small compared to the intrinsic ambiguity in assigning types with the available images. The comments included in Tables 4a-k not only describe important features that went into the classification, but also record the uncertain features that resulted in significant disagreements between classifiers, for example "faint protrusions top and bottom, or disk?" or "spiral arms barely visible?" In summary, the majority of the morphological classifications are reliable to better than one class, but in a few, predominantly fainter cases, where features such as disks and arms are at the limit of detectability, the uncertainty may be more than one class.
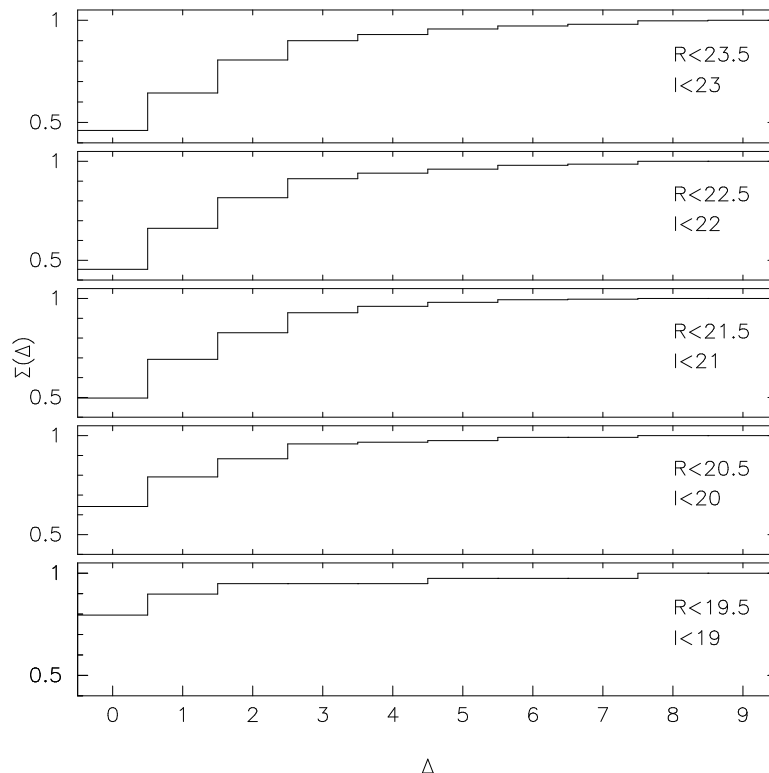
Figure 1. The cumulative distribution of the absolute differences in T types assigned to galaxies by independent pairs of classifiers. These are shown for a number of magnitude limits. The vertical scale of each plot runs from 40% to 100% in 10% steps. One class in the Revised Hubble scheme is roughly equivalent to 2-3 units on the T type scale. We achieve agreement within one Hubble class for more than 80% of galaxies down to our completeness limit.

The classifications from RSE are particularly important because of his central role in the typing of galaxies in the Medium Deep Survey (MDS; Griffiths et al. 1994), an intermediate-redshift "field" sample with which we wish to compare. For this reason we have been very critical in our comparison of differences between RSE's classification and the other 3 classifiers. We judged that, while the scatter between RSE and AD/WJC/AO is marginally larger than internal scatter of the latter group, there are no systematic differences between the RSE (MDS) system and the one adopted here. At the level of the published MDS classifications, which, for example, does not discriminate between E and S0 galaxies and the full range of subclasses of spirals, we believe that the data presented here can be considered to be on a consistent system with the MDS.

The estimates of the disturbance index and the dynamical state were merged by AD in a similar manner to the morphologies. The disturbance indices were found to agree to better than one unit, on average. The dynamical state is not continuous, nor has it been required that each classifier supply one. Indeed, we find that more often than not, in comparing pairs of observers, only ∼40% of cases are assigned a dynamical state by both. Of these, however, the classifiers agree on the descriptive index more than 60% of the time, far better than the chance occurence of 25%. The fact that most objects were not flagged for comment is a clear indication of the subjectivity of this index, but, at the same time, the agreement of the assigned category suggests that something genuine is being quantified in cases of obvious disturbance.

The final assignments of revised Hubble types were converted to de Vaucouleurs "T types" as coded in Table 2b of the Second Reference Catalog of Bright Galaxies (de Vaucouleurs, de Vaucouleurs, and Corwin 1976). The main Hubble types are: D/cD, -7; E, -5; S0, -2; Sa, 1; Sb, 3; Sc, 5; Sd, 7; Sm, 9 and Irr, 10 (note -1 is not used). The full morphological information on our cluster fields is given in Tables 4a-k.
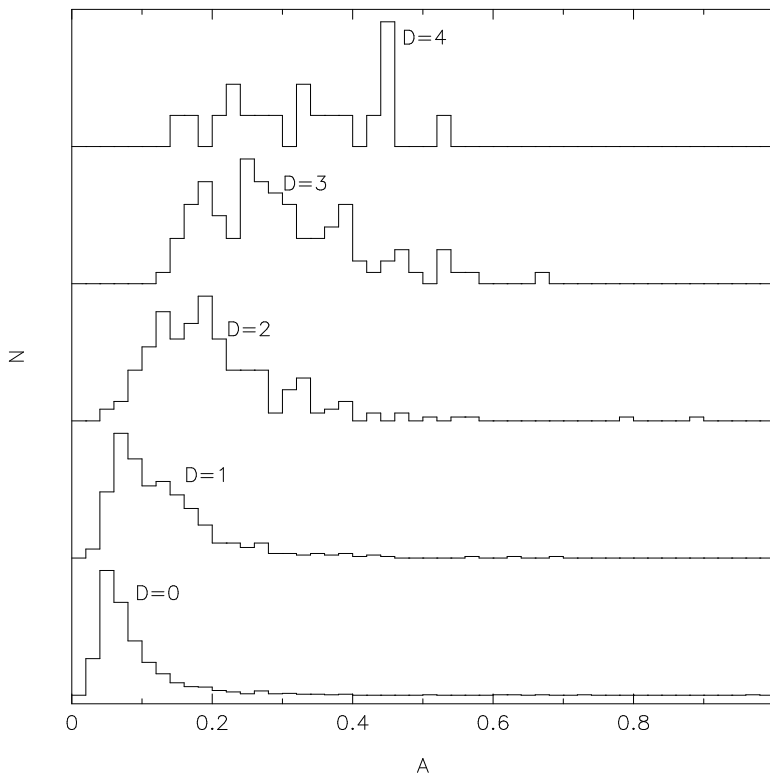
Figure 2. The distribution of the algorithmically determined asymmetry parameter (A) at a given value of the disturbance index (D). There is obviously a good correlation between the two parameters. The scatter at a fixed disturbance index is similar in magnitude to the difference between successive disturbance bins, supporting the resolution of the adopted disturbance scale.

In addition to the visual estimates of morphological disturbance determined from these samples, we have also measured a simple quantitative index of image asymmetry. This index measures the proportion of light in a galaxy in an asymmetric component compared to the total luminosity. Operationally we determine this value by rotating the galaxy by 180 degrees around its intensity-weighted centroid and subtracting this rotated image from the original. The subtracted image is then smoothed with a 0.2 arcsec diameter top-hat filter and the positive flux within the original detection isophote summed, the ratio of this to the total isophotal flux of the galaxy gives the asymmetry parameter (A).

3.2. Comparison of Visual and Machine-based Parameters

In this section we compare various visually determined properties of galaxy morphology with the equivalent algorithm-derived parameter to highlight the strengths and weaknesses of the two approaches.
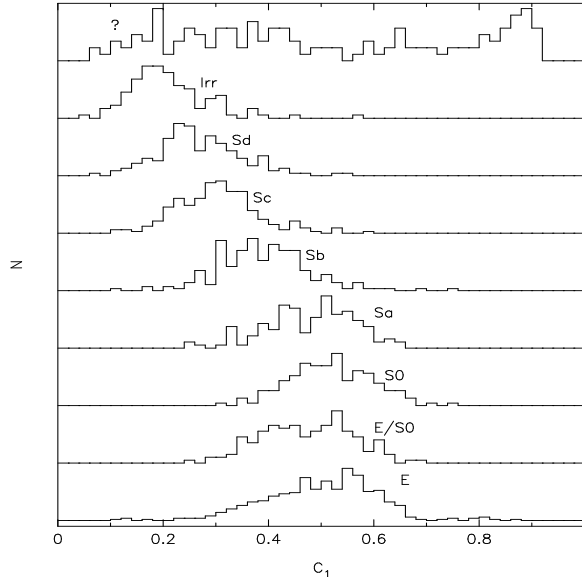
Figure 3. The distribution of the concentration index (C_1) for different morphological types showing the good correlation between bulge-to-disk ratio (crudely measured by C_1) and type for spiral galaxies. For morphological types of Sa and earlier, however, the concentration index fails to provide any useful differentiation. The histogram at the top of the plot shows the distribution of C_1 for unclassified and compact objects on the frames.

We start by showing in Fig. 2 the distribution of the asymmetry parameter (A) for different values of the visually-determined disturbance index (D). There appears to be a good correlation between these two, and furthermore the scatter in the asymmetry for a given value of the disturbance index supports the resolution adopted in our scheme. The only instance where the disturbance index obviously out-performs the quantitative asymmetry is when there are close companions to the galaxy (lying within the detection isophote of the object) or when the galaxy lies on a background with a strong gradient. Both of these are particularly a problem for the case of the "additional" objects (ID > 3000) which have been deblended by hand and for this reason we suggest the asymmetry index for such object should be treated with caution.

Figure 3 shows the distribution of the concentration index (C_1) as a function of Hubble type for the full morphological sample. This comparison, as well as that between the algorithm-based asymmetry parameter and the visual disturbance index shown in Fig. 2, illustrates both the strengths and weaknesses of algorithm-based classifications. In particular, the concentration index, as used here, becomes a useless discriminator for types Sa and earlier, which have virtually identical distributions of this quantity over a substantial range in morphology. Additional information from other simple algorithm-based parameters (e.g. asymmetry) would obviously not remove this failure. This highlights the importance of more sophisticated morphological parameterization, including visual inspection, in understanding the evolution of galaxy structure and stellar populations.
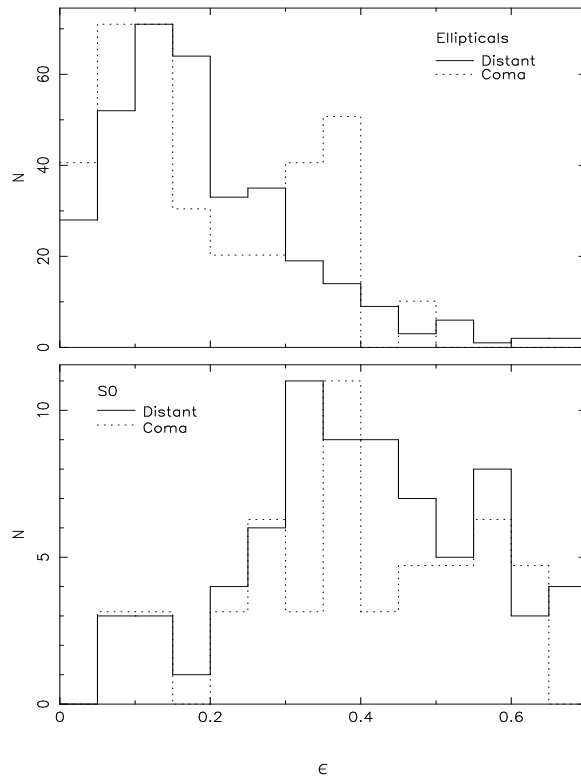
Figure 4. The ellipticity distributions for E and S0 galaxies in the distant clusters (solid histogram) compared to equivalent samples drawn from the Coma cluster from Andreon et al. (1996; dotted histogram). We find good agreement between the shapes of the distributions within each morphological type. A more extensive comparison with the equivalent distributions from the Revised Shapley-Ames catalog (Sandage, Freeman & Stokes 1970) and the cluster catalog of Dressler (1980), both based on high-quality plate material, indicate that at worst we are missing $\lesssim 50\%$ of the face-on S0 galaxies (those with $\epsilon \leq 0.3$) amounting to $\sim 12\%$ of the total population. The ordinate gives the number of galaxies in each bin in the distant cluster sample, the samples from Coma have been rescaled to the same peak.

The discrimination between E and face-on S0 galaxies has been a tradition concern in morphological classification. While it is desirable that this distinction exactly follow the definition of the Revised Hubble system, which for face-on S0 galaxies means the ability to discern a more extended outer envelope than would be seen for an elliptical galaxy, it is equally important for our purposes that our classifications be consistent with similar studies, particularly those of low-redshift clusters imaged on photographic plates or with CCDs. Accordingly, we have attempted to estimate the degree of incompleteness in our S0 classification due to our missing face-on systems by comparing the ellipticity distributions of our distant E and S0 galaxies with similar samples from both local rich clusters and the field. Perhaps the best sample for this purpose is the CCD survey of Coma galaxies by Andreon et al. (1996) who provide axial ratios for a magnitude-limited sample of ~ 100 galaxies in the central regions of Coma. These are CCD images, like those used here, measured at the $\mu_R = 24.0$ mags arcsec^{-2} isophote. With $(1 + z)^4$ dimming and K corrections applied this isophote is equivalent to that used in our analysis of the distant clusters, and due to the ~ 2 mag darker sky as seen from space, the contrast of this isophote with the sky is nearly the same for the Andreon sample as our own HST sample. We show the distributions for the galaxies in Coma and our distant clusters in Fig. 4. A two sample Kolmogorov-Smirnov gives a 42% probability that the distant ellipticals and those in Coma have

the same ellipticity distribution, while the S0 samples agree at an even higher level (88%). Hence at least from this comparison there is no strong evidence of an enhanced deficit of round face-on S0's or a corresponding increase in the proportion of round ellipticals in our catalogs compared to similar samples of local clusters.

In terms of the absolute numbers of face-on S0's, the comparison given above is misleading, in that Andreon et al. (1996) are probably also missing a fraction of the face-on S0's in their sample. This conclusion comes from taking the simplest model of S0's as randomly-projected thin disks, which would predict a flat distribution of numbers of S0's with ellipticity. To further investigate this we have chosen to compare the fraction of round (arbitrarily chosen to be $\epsilon \leq 0.3$) S0's in our catalog with the equivalent values from the Revised Shapley-Ames catalog (Sandage, Freeman & Stokes 1970; SFS) and the cluster catalog of Dressler (1980), both based on very high-quality plate material. We find $23 \pm 6\%$ of our S0's have $\epsilon \leq 0.3$, compared to $33 \pm 4\%$ for SFS and $34 \pm 3\%$ for Dressler (1980). While not statistically significant, our value is lower than these two measurements and would indicate that we could be missing up to 40–50% of the face-on S0's, or 12% of the total S0 population. This would seriously compromise the use of our catalog for determining the intrinsic shapes of the S0 population in our distant clusters (c.f. SFS), but does not substantially change the proportion of S0's in the clusters. In summary, it seems likely that our sample *is* deficient in face-on S0 galaxies compared with a pure application of the Revised Hubble system, but that this deficiency is shared by most of the work involving the morphological classification of all but the nearest galaxy clusters.

4. Cluster Galaxy Populations

We now present some basic properties of the galaxy populations in the clusters discussed here. We primarily discuss the morphological composition of the clusters amd then touch briefly on a number of areas which are dealt with in more depth in other publications.

We first discuss the morphological mixes in the distant clusters to a fixed absolute magnitude, $M_V = -17.5 + 5 \log h$. Before doing this, however, we have to correct the samples for field contamination. Here we rely on the extensive morphological survey of faint field galaxies by the MDS team. Using the catalogs kindly provided to us by the MDS team we have fitted power laws to the differential number counts as a function of morphological type to $I_{814} = 22.0$. For the E and S0 subclasses (which are combined in the published MDS results) we use the classifications from RSE which include these classes. These are then used in each of the cluster fields (extrapolating slightly when necessary) to estimate the contamination from field galaxies (and its morphological mix) in our catalogs. At $I_{814} = 23.0$ we estimate the field contamination is ~ 11.2 galaxies/arcmin^2, equivalent to 60 galaxies per WFPC-2 field. The rough breakdown into morphological classes is: E, 10%; S0, 10%; Sab, 25%; Scdm, 30% and Irr, 25%. These field distributions are then subtracted from the cluster morphological distributions (assuming flat distributions in T type within each of the larger MDS classification bins). We show the field-corrected distributions of galaxy morphology brighter than $M_V = -17.5 + 5 \log h$ in our

clusters in Fig. 5. The absolute magnitudes of the galaxies are determined from their "Kron" magnitudes (variable-diameter aperture magnitudes whose size depends upon the galaxy scale size, see Bertin & Arnouts (1996) and also Kron (1980)), assuming that they lie at the cluster redshift. We then use the relevant non-evolving spectral energy distribution for the observed morphological type to estimate the K correction. This ignores any possible luminosity dependence of the K correction within a morphological class. This effect should be negligible as we are estimating luminosities from passbands which sample close to restframe V. Taking the ellipticals as an example we expect the variation in K correction as a function of galaxy luminosity will lead to an error in the estimated luminosity of less than 1% across the range covered by our samples.

The most immediate features of the distributions shown in Fig. 5 are the dominant population of elliptical galaxies (T type -5) seen in the central fields and the decline in the prevelance of this population in the outskirts of the clusters (as indicated by the distributions for the two outer fields imaged in our survey; A370#2 and Cl0939+47#2). It is obvious that even at a redshift of $z \sim 0.5$ the dominant bright galaxy component in the cores of rich clusters are morphologically identifiable as elliptical galaxies. Furthermore, we also find that within the core fields the ellipticals are concentrated around the cluster centers, with an average radial surface density profile fitted by $\Sigma(r) \propto r^\gamma$ with $\gamma = -0.80 \pm 0.10$ out to 200 h^{-1} kpc, close to an isothermal profile. The profile is calculated around the cluster centers as indicated by the lensing shear field (Smail et al. 1996) and has been corrected for uniform field contamination. The evolution of the "morphology-density" and "morphology-radius" relations are discussed in detail in Dressler et al. (1996).
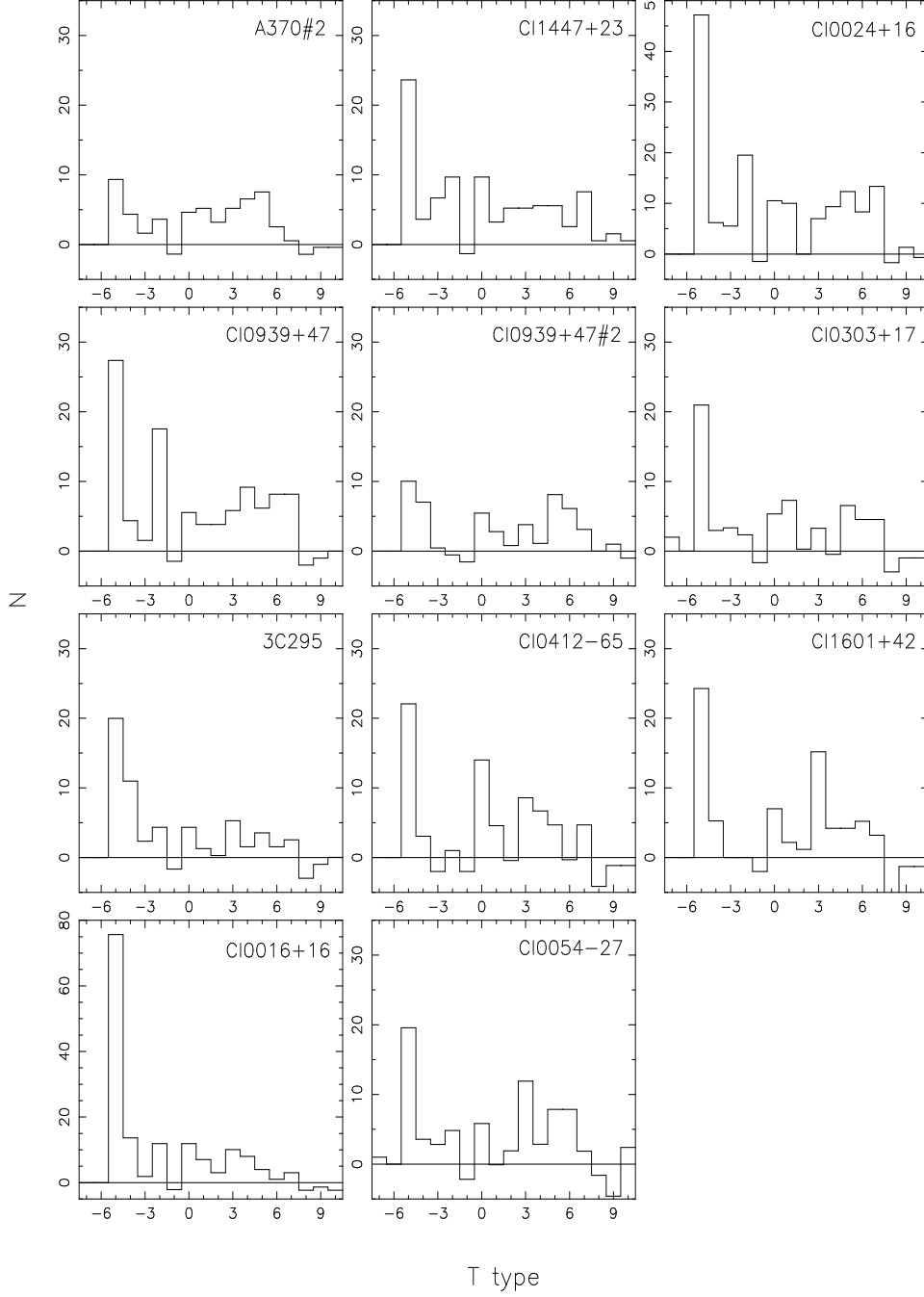
Figure 5. The distribution of galaxy morphology expressed as T types, brighter than $M_V = -17.5 + 5 \log h$ in our 11 fields, 9 central fields and the 2 outer fields A370#2 and Cl0939+47#2. These have been corrected for reddening and then field contamination using the morphologically classified field counts from the MDS. Note the different vertical scales on some plots.

We plot the luminosity function of the elliptical populations in our clusters in Fig. 6. The galaxy luminosities and field corrections have been estimated in the same manner as was used for the morphological mixes. The luminosity functions have then been combined into 3 independent

redshift bins: A370#2, Cl1447+23 and Cl0024+16 with $<z>=0.38$; Cl0939+47, Cl0939+47#2, Cl0303+17 and 3C295 with $<z>=0.43$; Cl0412−65, Cl1601+42, Cl0016+16 and Cl0054−27 with $<z>=0.54$. Fitting a standard Schechter function to these distributions, with a fixed faint end slope of $\alpha = -1.25$, we obtain characteristic luminosities of $M_V^* = -20.47 \pm 0.18 + 5\log h$ at $<z>=0.38$, $M_V^* = -20.62 \pm 0.13 + 5\log h$ ($<z>=0.43$) and $M_V^* = -20.76 \pm 0.12 + 5\log h$ for $<z>=0.54$. These fits are shown overlaid on Fig. 6 and the quoted limits include the uncertainty in the field contribution to the counts. For a low redshift comparison we take the analysis by Colless (1989) of 14 rich clusters, where he derives $M_{b_j}^* = -19.84 \pm 0.06 + 5\log h$ for $\alpha = -1.25$, or $M_V^* \sim -20.5 + 5\log h$ assuming a mean color of $(b_j - V) \sim 0.7$. Thus, there appears to be a slow, but significant brightening of the population between $z = 0.0$–0.54 amounting to at least $\delta M_V \sim -0.3$. This brightening is consistent with observations of the homogeneity of the colors of these galaxies (Ellis et al. 1996) and their luminosity-size relationship (Barger et al. 1996), both of which indicate that the bulk of the stars in this population were formed at very early epochs.

Figure 6 shows that although we have not allowed the faint end slope of the elliptical population to vary it does appear to be reasonably described by the local value of $\alpha \sim -1.25$. We highlight this because of recent discussions of the relative importance of age and metallicity effects in defining the color-magnitude relation of cluster elliptical galaxies (Worthey 1994; Kodama & Arimoto 1996). If age differences are assumed to cause the trend of fainter ellipticals being bluer then Kodama & Arimoto (1996) found that to adequately describe the local color-magnitude relation L^* ellipticals are still forming at $z \sim 0.2$–0.3 ($h = 0.5$ and $q_o = 0.5$). They point out that the color evolution implied by this model is incompatible with the observed form of the color-magnitude relation in distant clusters. Equally, in such a model the bulk of the elliptical population fainter than $\sim L^*$ would not be present in the most distant clusters we observe. We would thus expect the ratio of the numbers of low and high luminosity ellipticals to be considerably lower than in local clusters, corresponding to a shallower faint end slope. The absence of any strong change in α for ellipticals brighter than $L_V \sim L^* + 3$ out to $z \sim 0.6$ would appear to contradict this. We thus confirm Kodama & Arimoto's conclusion that age variations are unlikely to be the dominant cause of the color-magnitude relation of ellipticals in rich clusters.

Returning to Fig. 5 we also note that the clusters contain only small populations of S0 galaxies ($\sim 15\%$). We have shown in Fig. 4 that this is unlikely to have resulted from a widespread misclassification of S0's as elliptical galaxies, although our misclassification of face-on S0's will lead to an increase in the total S0 population by $\sim 12\%$ – raising the fraction of S0 galaxies to $\sim 17\%$ of the total cluster population. The absence of the S0 population is thus particularly intriguing, given that they constitute $\sim 40\%$ of local clusters. Unfortunately, with so few S0's it is impossible to obtain adequate numbers to measure the luminosity function and its evolution within our sample. The small fractions of S0's in our clusters and the implications of this for their formation and evolution is outside the scope of the discussion here and we return to it elsewhere (Dressler et al. 1996). We note that the S0's lie intermediate between the ellipticals and the spirals (see below) in their radial distribution, with $\gamma = -0.59 \pm 0.15$ interior to 200 h^{-1} kpc.

Moving to later Hubble types we see that all clusters contain populations of these systems. The field-corrected spiral fraction in the clusters (the fraction of the total population which have

morphologies of Sa or later) is listed in Table 1. The radial profile of these galaxies around the cluster centers is substantially shallower than the elliptical population, dropping only as $\gamma = -0.29 \pm 0.08$, as expected for a dynamically unrelaxed component of the clusters. Following our earlier discussion we plot the combined luminosity function of the cluster spirals (Sa's and later, identified statistically by subtracting the field counts from the MDS) in Fig. 7. Again fitting a Schechter function, this time with $\alpha = -1.0$, we see no evidence for change between the different epochs, in contrast to the elliptical populations. We find $M_V^* = -20.19 \pm 0.18 + 5 \log h$ at $<z>= 0.38$, $M_V^* = -20.17 \pm 0.15 + 5 \log h$ ($<z>= 0.43$) and $M_V^* = -20.21 \pm 0.15 + 5 \log h$ for $<z>= 0.54$. We compare these with the parametrisation of the field galaxy luminosity function by Lilly et al. (1995), which is dominated by spiral galaxies. They find $\alpha = -1.0$ and $M_B^* \sim -19.4 + 5 \log h$ for galaxies brighter than $M_B^* < -17.2 + 5 \log h$ in the redshift range $z = 0.2$–0.5, roughly equivalent to that probed here. Taking a mean restframe color of $(B - V) \sim 0.6$ for this population we have $M_V^* \sim -20.0 + 5 \log h$, very close to that found in our sample. Given the differences in the photometric systems used in the cluster and field surveys, as well as the different sample selection criteria, we feel that it is too early yet to claim a systematic difference between the luminosities of spiral galaxies in distant clusters and the surrounding field.

Although the HST images discussed here provide excellent photometry, with small photometric errors for even the fainter galaxies (thanks to the significantly darker sky background from space), uncertainties in the luminosity functions derived for the clusters remain large because of the substantial contamination by foreground and background galaxies — a much more significant problem than for nearby clusters. The advent of the new generation of large, ground-based telescopes will considerably improve the situation by providing extensive membership information for galaxies in these fields. With large samples of confirmed cluster members it will be possible to robustly measure the evolutionary brightening of the elliptical population, while comparison of the luminosity function of spiral members with that derived for the field will indicate whether there are any substantial differences between these two populations. Such an effort, though intensive of telescope time, would be very worthwhile.
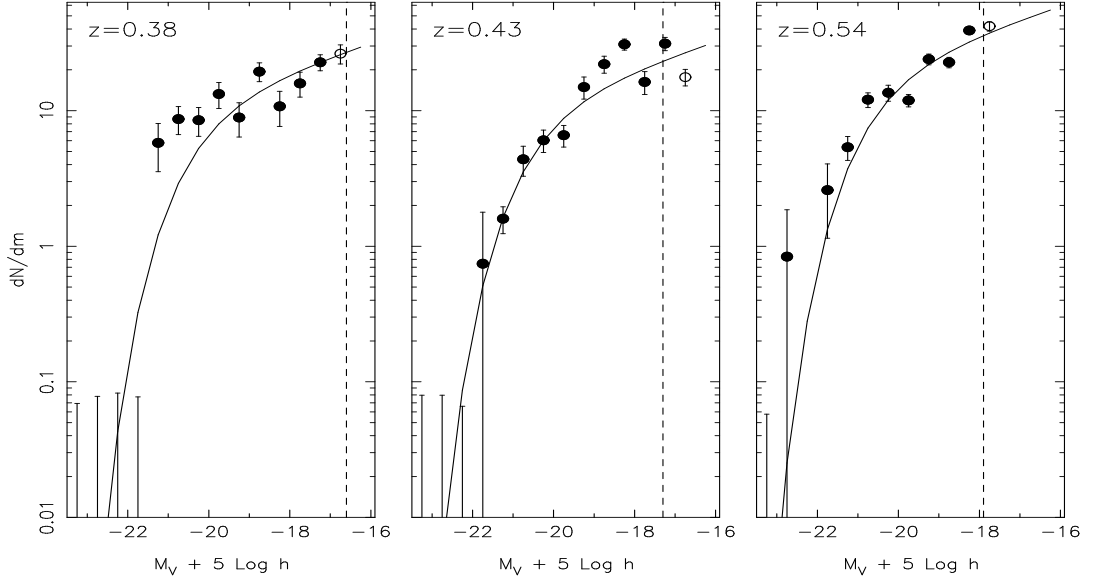
Figure 6. The luminosity function of cluster elliptical galaxies in three redshift bins. The counts are corrected for field contamination and then converted to absolute V magnitudes assuming K corrections for a non-evolved elliptical spectral energy distribution. Overlayed on these are the best fitting Schechter function (with a fixed $\alpha = -1.25$ faint end slope). Points with filled symbols are used in the fitting. The dashed line shows the magnitude limit for the samples.
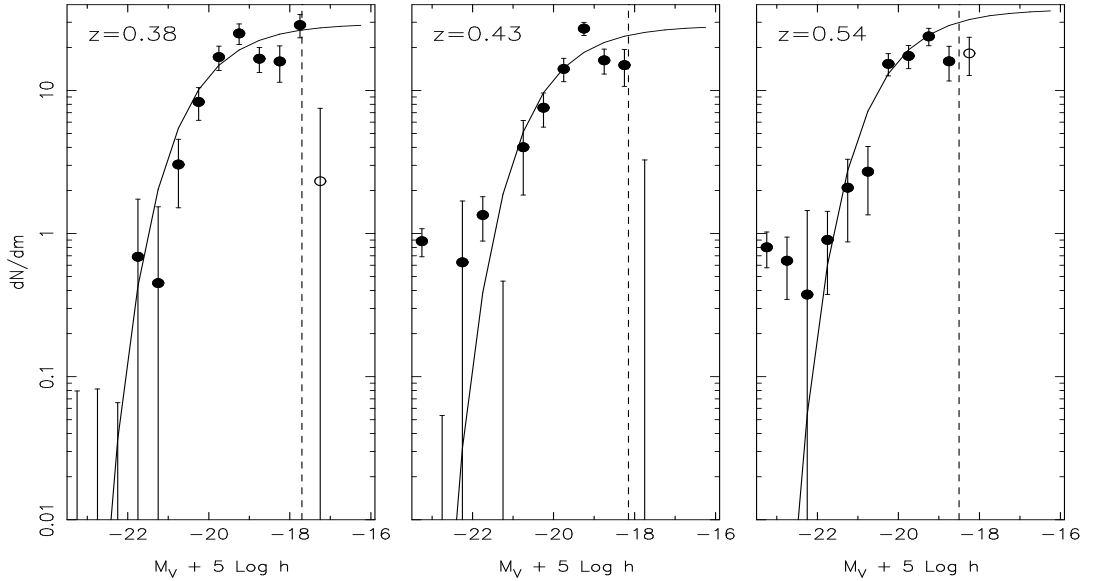
Figure 7. The luminosity function of cluster spiral galaxies in three redshift bins (the same as those used in Fig. 6). The counts are corrected for field contamination and then converted to absolute V magnitudes assuming K corrections for the relevant non-evolved spectral energy distribution of each morphological sub-type. Overlayed on these are the best fitting Schechter function (with a fixed $\alpha = -1.0$ faint end slope). Points with filled symbols are used in the fitting. The dashed line shows the magnitude limit for the samples.

Acknowledgements

REFERENCES

Abrahams, R.G., Valdes, F., Yee, H.K.C. & Van den Bergh, S., 1995, ApJ, 432, 75.

Andreon, S., Davoust, E., Michard, R., Nieto, J.-L. & Poulain, P., 1996, A&AS, 116, 429.

Barger, A.J., Aragón-Salamnaca, A., Smail, I., Ellis, R.S., Couch, W.J., Dressler, A., Oemler, A., Butcher, H. & Sharples, R.M., 1996, in prep.

Bertin E. & Arnouts, S., 1996, A&A, in press.

Broadhurst, T.J., Ellis, R.S. & Shanks, T., 1988, MNRAS, 235, 827.

Butcher, H. & Oemler, A., 1978, ApJ, 279, 18.

Butcher, H. & Oemler, A., 1984, ApJ, 285, 426.

Castander, F.J., Ellis, R.S., Frenk, C.S., Dressler, A. & Gunn, J.E., 1994, ApJ, 424, L79.

Colless, M.M., 1989, MNRAS, 237, 799.

Couch, W.J. & Sharples, R.M., 1987, MNRAS, 229, 423.

Couch, W.J., Ellis, R.S., Sharples, R.M. & Smail, I., 1994, ApJ, 430, 121.

Cowie, L.L., Songaila, A. & Hu, E.M., 1996, preprint.

de Vaucouleurs, Z., de Vaucouleurs, Z. & Corwin, H., 1976.

Dressler, A., 1980, ApJS, 42, 565.

Dressler, A. & Gunn, J.E., 1992, ApJS, 78, 1.

Dressler, A., Oemler, A., Butcher, H. & Gunn, J.E., 1994, ApJ, 430, 107.

Dressler, A., Oemler, A., Smail, I., Couch, W.J., Ellis, R.S., Barger, A., Butcher, H., Poggianti, B.M. & Sharples, R.M., 1996, ApJ, submitted.

Ellis, R.S., Smail, I., Dressler, A., Couch, W.J., Oemler, A., Butcher, H. & Sharples, R.M., 1996, ApJ, submitted.

Griffiths, R.E., Casertano, S., Ratnatunga, K.U., Neuschaefer, L.W., Ellis, R.S., Gilmore, G.F., Glazebrook, K. Santiago, B., Huchra, J.P., et al., 1994, ApJ, 435, L19.

Henry, J.P., Soltan, A., Briel, U. & Gunn, J.E., 1982, ApJ, 262, 1.

Holtzman, J.A., Burrows, C.J., Casterno, S., Hester, J.J., Trauger, J.T., Watson, A.M. & Worthey, G., 1995, PASP, 107, 1065.

Kodama, T. & Arimoto, N., 1996, preprint (astro-ph/9609160).

Kron, R.G., 1980, ApJS, 43, 305.

Lilly, S.J., Tresse, L., Hammer, F., Crampton, D. & LeFevre, O., ApJ, 1995, 455, 108.

Oemler, A., Dressler, A. & Butcher, H., 1996, ApJ, submitted.

Sandage, A., Freeman, K.C. & Stokes, R.A., 1970, ApJ, 160, 831. (SFS)

Soucail, G., Mellier, Y., Fort, B. & Cailloux, M., 1988, A&AS, 73, 471.

Smail, I., Ellis, R.S., Dressler, A., Couch, W.J., Oemler, A., Butcher, H. & Sharples, R.M., 1996, ApJ, in press.

Wang, Q.D. & Stocke, J.T., 1993, ApJ, 408, 71.

Worthey, G., 1994, ApJS, 95, 107.

PLATE CAPTIONS

Plate 1a. Field of A370#2.

Plate 1b. Field of Cl1447+23.

Plate 1c. Field of Cl0024+16.

Plate 1d. Field of Cl0939+47.

Plate 1e. Field of Cl0939+47#2.

Plate 1f. Field of Cl0303+17.

Plate 1g. Field of 3C295.

Plate 1h. Field of Cl0412−65.

Plate 1i. Field of Cl1601+42.

Plate 1j. Field of Cl0016+16.

Plate 1k. Field of Cl0054−27.

TABLE 1

CLUSTER SAMPLE AND PROPERTIES

Cluster	R.A. (J2000)	Dec. (J2000)	P.A. V3 (deg)	z	T_{exp} (ks)				L_X(0.3–3.5) h^{-2} 10^{44} ergs	σ km/s [N]	kpc/arcsec (h^{-1})	E(B-V)	$\mu(1\sigma)$	N Morph	All	f_{sp}
					F450W	F555W	F702W	F814W								
A370#2	02 40 01.1	−01 36 45	235.00	0.37	...	8.0	...	12.6	2.73	1350 [34]	3.09	0.01	27.5	129	542	0.54
Cl1447+23	14 49 28.2	+26 07 57	125.35	0.37	...	...	4.2	...	...	...	3.09	0.02	27.5	210	792	0.47
Cl0024+16	00 26 35.6	+17 09 43	328.30	0.39	23.4	...	...	13.2	0.55	1339 [33]	3.17	0.03	27.5	248	835	0.40
Cl0939+47	09 43 02.6	+46 58 57	47.32	0.41	...	...	21.0	...	1.05	1081 [31]	3.26	0.00	27.3	207	975	0.46
Cl0939+47#2	09 43 02.5	+46 56 07	315.00	0.41	...	4.0	...	6.3	1.05	1081 [31]	3.26	0.00	26.9	116	627	0.62
Cl0303+17	03 06 15.9	+17 19 17	50.13	0.42	...	...	12.6	...	1.05	1079 [21]	3.29	0.12	27.9	161	891	0.46
3C295	14 11 19.5	+52 12 21	282.04	0.46	...	...	12.6	...	3.20	1670 [21]	3.43	0.00	27.1	142	899	0.28
Cl0412−65	04 12 51.7	−65 50 17	174.00	0.51	...	12.6	...	14.7	0.08	...	3.59	0.00	27.5	155	865	0.47
Cl1601+42	16 03 10.6	+42 45 35	315.00	0.54	...	...	16.8	...	0.35	1166 [27]	3.67	0.00	28.3	145	928	0.46
Cl0016+16	00 18 33.6	+16 25 46	250.00	0.55	...	12.6	...	16.8	5.88	1703 [30]	3.67	0.03	26.7	211	837	0.21
Cl0054−27	00 56 54.6	−27 40 31	121.00	0.56	...	12.6	...	16.8	0.25	...	3.72	0.00	27.4	133	767	0.42

TABLE 2A

NOTES ON PARAMETERS IN TABLE 3

Column	Heading	Parameter	Units	Format	Comment
1	ID	NUMBER		i4	Object identifier[1]
2	X	X_IMAGE	pixels	f8.2	X centroid on frame
3	Y	Y_IMAGE	pixels	f8.2	Y centroid on frame
4	I_{814}^{ap}	F814W_APER	mags	f7.3	1.0$''$ diameter aperture magnitude[2]
5	δI_{814}^{ap}	F814W_ERR_APER	mags	f7.3	Error on above
6	I_{814}^{iso}	F814W_ISO	mags	f7.3	Isophotal magnitude above detection isophote
7	δI_{814}^{iso}	F814W_ERR_ISO	mags	f7.3	Error on above
8	I_{814}^{best}	F814W_BEST	mags	f7.3	Optimal measure of total magnitude[3]
9	δI_{814}^{best}	F814W_ERR_BEST	mags	f7.3	Error on above
10	Area	ISOAREA_IMAGE	pixels	i5	Isophotal area above detection isophote
11	r_k	KRON_RADIUS	pixels	f6.2	Kron radius
12	a	A_IMAGE	pixels	f6.2	2nd order moment along the major axis
13	b	B_IMAGE	pixels	f6.2	2nd order moment along the minor axis
14	θ	THETA_IMAGE	degrees	f6.1	Orientation of major axis[4]
15	μ_{thresh}	MU_THRESHOLD	mags arcsec^{-2}	f7.3	Detection threshold
16	μ_{max}	MU_MAX	mags arcsec^{-2}	f7.3	Peak surface brightness
17	Sky	BACKGROUND	DN	f8.2	Sky background level
18	FWHM	FWHM_IMAGE	pixels	f6.2	FWHM from gaussian fit
19	P_{star}	CLASS_STAR		f5.2	Star-galaxy classification[5]
20	C_1	CONC		f6.3	Concentration index[6]
21	C_2	CONTRAST		f5.2	Contrast index[6]
22	Err	FLAGS		i4	Error flags[7]
23	$V_{555} - I_{814}$	F555W−F814W	mags	f7.3	Color measured in a 1.0$''$ diameter aperture[8]
24	$\delta(V_{555} - I_{814})$	F555W−F814W_ERR	mags	f7.3	Error on above[8]

Table 2b

Notes on parameters in Table 4

Column	Heading	Parameter	Format	Comment
1	ID	NUMBER	i4	Object identifier[1]
2	DG #	DG_NUMBER	a3	Cross identification to DG92[9]
3	I_{814}	F814W_BEST	f7.3	Optimal measure of total magnitude[2,3]
4	A	ASYMMETRY	f6.3	Asymmetry parameter[10]
5	Class	MORPHOLOGY	a12	Hubble class[11]
6	T-type	T_TYPE	i3	T-type[12]
7	D	DISTURBANCE	i3	Disturbance index[13]
8	Int	INTERPRETATION	a8	Interpretation of disturbance[14]
9	Comments	COMMENTS	a62	Description of object morphology

1 ID's starting 2000 denote objects lying on the PC chip,
   those starting from 3000 are "additional" objects lying on the WFC (see text).
2 Parameter is F702W where applicable.
3 Variable-diameter aperture magnitude measured in an elliptical aperture of major axis radius $2.5r_k$, unless
   Err=1 occured in which case it the "corrected" isophotal magnitude is used (Bertin & Arnouts 1996).
4 Defined counter-clockwise from the positive X axis in the range -90 to 90.
5 Star-galaxy classifier using neural-net weights: 0.0 denotes a galaxy and 1.0 a star.
6 See text for details.
7 Error flag values and the associated error are quoted below:

$\quad$ 1 $\quad$ — bright neighbors may bias magnitude estimate,
$\quad$ 2 $\quad$ — originally a blend,
$\quad$ 4 $\quad$ — saturated,
$\quad$ 8 $\quad$ — object truncated by frame boundary,
$\quad$ 16 $\quad$ — incomplete aperture photometry,
$\quad$ 32 $\quad$ — incomplete isophotal photometry,
$\quad$ 64 $\quad$ — memory overflow during deblending,
$\quad$ 128 $\quad$ — memory overflow during extraction.

8 Only for those fields with color information (F450W−F814W for Cl0024+16),
   a value of 99.999 in these fields denotes an undefined measurement.
9 Non-exhaustive cross identification of objects against the catalogs in Dressler & Gunn (1992),
   for the clusters Cl0024+16, Cl0939+47, Cl0303+17, 3C295, Cl1601+42 and Cl0016+16.
10 An error is denoted by a value of 9.999, values for "additional" objects should be
   viewed with caution.
11 The standard Hubble classification scheme (E, S0, Sa, Sb...) with the addition of:

$\quad$ D, cD $\quad$ — Morgan type D or cD galaxy,
$\quad$ E/S0 or S0/E $\quad$ — cannot distinguish E or S0,
$\quad$ X $\quad$ — compact object (likely non-stellar but too compact to see structure),
$\quad$ ∗ $\quad$ — stellar image,
$\quad$? $\quad$ — unclassifiable.

12 Standard T-type, an undefined entry is given as -99.
13 Disturbance index:

$\quad$ 0 $\quad$ — normal,
$\quad$ 1 $\quad$ — moderate asymmetry,
$\quad$ 2 $\quad$ — strong asymmetry,
$\quad$ 3 $\quad$ — moderate distortion,
$\quad$ 4 $\quad$ — strong distortion,
$\quad$ -99 $\quad$ — undefined.

14 Interpretation of disturbance classes:

$\quad$ M $\quad$ — merger,
$\quad$ I $\quad$ — tidal interaction with neighbor,
$\quad$ T $\quad$ — tidal feature,
$\quad$ C $\quad$ — chaotic,
$\quad$! $\quad$ — remarkable.

Y	I_{814}^{ap}	δI_{814}^{ap}	I_{814}^{iso}	δI_{814}^{iso}	I_{814}^{best}	δI_{814}^{best}	Area	r_k	a	b	θ	μ_{thresh}	μ_{max}	Sky	FWHM	P_{star}	C$_1$	C$_2$	Err	$V-I$	$\delta(V-I)$
2.58	25.840	0.187	26.198	0.133	26.011	0.174	9	4.36	0.92	0.77	85.2	24.600	22.947	30.19	2.68	0.01	0.228	0.64	24	99.999	99.999
5.21	26.007	0.244	26.159	0.132	25.887	0.180	10	4.17	1.07	0.81	17.5	24.600	23.170	30.12	5.56	0.01	0.101	0.57	16	99.999	99.999
4.20	25.306	0.128	25.515	0.103	25.085	0.144	17	5.00	1.84	1.34	-59.4	24.600	22.857	30.18	9.37	0.00	0.032	0.71	24	99.999	99.999
5.95	22.511	0.017	22.182	0.016	22.123	0.017	140	4.17	4.11	1.67	27.3	24.600	20.989	30.78	9.01	0.02	0.283	0.74	24	1.347	0.041
11.73	25.497	0.157	26.278	0.149	25.346	0.175	11	6.27	1.34	0.80	-37.9	24.600	23.322	30.26	4.94	0.00	-0.002	0.64	0	2.351	0.699
8.34	24.263	0.056	23.913	0.046	23.568	0.059	75	4.33	4.11	1.76	-37.7	24.600	22.972	30.22	16.09	0.00	0.135	0.52	24	1.018	0.106
4.99	20.123	0.005	20.080	0.005	20.121	0.005	167	3.50	1.59	1.31	12.2	24.600	16.524	30.19	1.43	0.95	0.818	0.95	24	2.684	0.018
10.39	24.349	0.060	24.544	0.060	24.107	0.072	37	4.83	1.85	1.52	62.0	24.600	22.437	30.33	5.23	0.00	0.207	0.64	0	1.840	0.220
17.81	25.628	0.176	25.951	0.121	25.592	0.130	14	3.69	1.49	0.67	-61.2	24.600	23.185	30.16	4.95	0.00	0.097	0.59	0	0.516	0.307
19.94	25.400	0.144	26.454	0.172	25.230	0.172	7	6.71	1.44	0.79	88.2	24.600	22.938	30.31	4.81	0.02	0.064	0.84	0	2.109	0.654
19.29	25.412	0.146	25.694	0.109	25.351	0.150	14	5.10	1.56	0.74	-80.1	24.600	22.511	30.78	6.43	0.10	0.144	0.82	0	2.758	1.038
23.99	25.277	0.130	25.744	0.109	25.073	0.130	15	6.00	1.46	0.72	-32.5	24.600	22.970	30.28	4.43	0.00	0.251	0.68	0	0.696	0.202
24.57	25.603	0.172	26.289	0.151	25.617	0.162	10	4.64	1.19	0.84	85.8	24.600	23.392	30.25	4.30	0.00	0.173	0.68	0	0.705	0.261
26.30	25.481	0.154	26.393	0.159	25.337	0.151	9	6.04	0.94	0.91	-75.0	24.600	23.618	30.12	5.05	0.00	0.145	0.62	0	1.566	0.405
23.55	23.903	0.043	23.910	0.042	23.681	0.058	54	4.72	2.23	1.73	-41.7	24.600	21.734	30.25	5.56	0.02	0.240	0.68	1	1.129	0.089
17.36	23.089	0.024	22.488	0.021	22.330	0.027	191	4.43	5.90	2.07	-62.5	24.600	21.809	30.23	16.88	0.00	0.246	0.65	24	0.802	0.041
25.49	22.318	0.015	22.034	0.014	21.966	0.016	157	3.96	3.61	1.87	-44.3	24.600	20.710	30.18	6.68	0.02	0.344	0.71	0	0.911	0.027
28.97	23.618	0.035	23.626	0.032	23.502	0.038	50	4.36	2.04	1.18	-52.9	24.600	21.018	30.46	3.41	0.02	0.342	0.72	0	1.270	0.085
33.22	24.383	0.062	24.448	0.052	24.377	0.068	32	4.20	1.84	1.00	-80.0	24.600	21.908	30.34	4.84	0.02	0.222	0.65	0	0.752	0.126
34.29	21.844	0.011	21.767	0.012	21.772	0.012	115	3.50	2.25	1.54	-74.9	24.600	19.339	30.16	2.70	0.02	0.532	0.83	0	0.914	0.021
.	.				.			.			.			.			.			.	.
.	.				.			.			.			.			.			.	.
.	.				.			.			.			.			.			.	.

TABLE 4A**

SAMPLE MORPHOLOGY CATALOG FOR A370#2

ID	DG #	I_{814}	A	Class	T-type	D	Int	Comments
4	...	22.123	0.052	Sc	5	0	...	highly inclined disk system; arms, structure visible?
7	...	20.121	9.999	*?	−99	−99	...	frame edge – star or bright object with jet
10	...	25.230	0.087	?	−99	−99	...	cosmic ray clump?
16	...	22.330	0.088	Sd	7	2	T	late type, with fan like extension toward frame edge
17	...	21.966	0.075	Sc	5	1	...	slightly wedge-shaped late type system
20	...	21.772	0.078	E/S0	−4	−99	...	small E or S0 – asymmetric and/or disturbed?
23	...	22.157	0.104	E	−5	0	...	small, highly concentrated spheroid or star
27	...	22.236	0.183	Sbc	4	2	...	mild warp, near edge-on disk and bulge; no perturber
30	...	22.373	0.104	Sc	5	0	...	edge-on late type; low SB
36	...	22.904	0.185	Sd/Irr	8	2	I?	late-type perturbed by nearby, concentrated dwarf
38	...	22.177	0.048	Sb/E?	3	2	T?	spiral w/ disturb disk, or E w/ tidal tails?
44	...	20.667	0.080	Sa	1	0	...	two smooth arm spiral with bulge; face on
46	...	22.785	0.162	Sc	5	2	...	small ring-like galaxy, chopped in two?
49	...	22.208	0.065	E/S0	−4	0	...	diffuse spheroid, or face on disk
54	...	22.105	0.055	E	−5	0	...	spheroid (distant?) with many surrounding companions
67	...	22.288	0.101	S0/a	0	1	...	S0 or spiral with asymetric disk
73	...	22.185	0.062	*	−99	−99	...	
75	...	20.833	0.258	Scd	6	3	M/I	2 tidal tails from merger, or interr w/ compan @11?
88	...	21.910	0.096	Sd/Sm	7	1	...	small, blobby disk
89	...	22.838	0.115	Sb	3	2	T?	tiny disk system, prominent bulge; spiral or tidal arm
.	.	.	.	.	.	.		
.	.	.	.	.	.	.		
.	.	.	.	.	.	.		

**Complete versions of Table 4 (Tables 4A–4K) are available on AAS CD-ROM series, Vol. ZZZ